Bulletin of Engineering Geology and the Environment (2024) 83:17
https://doi.org/10.1007/s10064-023-03515-7

ORIGINAL PAPER

A developed capillary tube model for suffossion susceptibility of non-cohesive soils

Ali Maroof[1] · Ahmad Mahboubi[1] · Eric Vincens[2] · Mojtaba Hassani[1]

Received: 5 July 2023 / Accepted: 5 December 2023 / Published online: 20 December 2023

Abstract

Pore geometrical models are widely used to study transport in porous media, permeability, internal stability, and filter compatibility. Transport of fine grains through the voids between the skeleton of the coarser fraction is mainly controlled by the pore throats or constriction sizes. This study compares various constriction size distribution criteria and capillary tube models, which elucidate the limitations of the Kovacs capillary tube model, and this model is explained and developed. The new proposed threshold boundaries ($d_0 = 2.3d^f_{85}$ and $d_0 = 2.8d^f_{85}$) categorized soil samples as internally stable, transient zone, or unstable. The model also incorporates the precise shape coefficient of particles. This improved model was validated based on a database from the literature, as well as performing 10 new experimental tests on two ideal gradation curves that identified the threshold boundary of Kenney and Lau criteria. This proposed model, which is dependent on grading, porosity, and grain shape, provides accurate predictions using a precise shape factor. This finding may enhance our knowledge about transport in porous media and contribute toward internal stability assessing for practical applications.

Keywords Internal stability · Suffusion · Controlling constriction size · Capillary tube model · Shape factor

Introduction

Pore geometry and its topology affect multiphase flow in porous media significantly. Network models can simulate the physics of air and fluid flow and mass transport in soil (Berkowitz and Ewing 1998). The coordination number is widely regarded as the main feature of network topology. The mean of the coordination number, the microscopic topology of pore connectivity, and its distribution should be determined using network models (Chatzis and Dullien 1977; Raoof and Hassanizadeh 2010). The soil structure and constriction size distribution (CSD) is one of the methods that can be used to estimate the fluid flow in porous media (Berkowitz and Ewing 1998; Sahimi 2011), permeability (Carman 1937; Fan et al. 2021),and the amount and size of eroded particles from the soil skeleton (Kezdi 1979; Kovacs 1981; Kenney et al. 1985; Indraratna and Vafai 1997).

The transport eventuality of granular media depends on the constriction size and its probability of occurring within the particles or constriction size distribution (Reboul et al. 2010). Transport of fine grains through the pores between the skeleton of coarser particles, under seepage flow, or vibrating force, is the major cause of instabilities of the granular assemblies, causing erosion phenomena (Kenney and Lau 1985). This phenomenon can occur when two basic conditions happen. Firstly, the pore diameter of the solid matrix should be greater than the smallest fine grains (geometrical conditions). If the first condition does not exclude fine-grain movement, then the hydraulic condition (critical velocity or hydraulic gradient) must be studied (Kovacs 1981; Wan and Fell 2008; Tangjarusritaratorn et al. 2022).

Common geometrical criteria for the internal stability assessment of cohesionless soils are a function of grain size and shape of the particle size distribution (Istomina 1957;

✉ Ahmad Mahboubi
a_mahboubi@sbu.ac.ir; ahmad.mahboubi@gmail.com

Ali Maroof
m_maroof@sbu.ac.ir

Eric Vincens
eric.vincens@ec-lyon.fr

Mojtaba Hassani
seyedmojtaba.hasani@yahoo.com

[1] Faculty of Civil, Water and Environmental Engineering, Shahid Beheshti University, Tehran 1658953571, Iran

[2] Ecole Centrale de Lyon, 36, Av Guy de Collongue, 69134 Ecully, France

Kezdi 1979; Kenney and Lau 1985; Burenkova 1993; Wan and Fell 2008; Chapuis 2021).

Furthermore, some geometrical criteria have been established based on soil structure/pore geometry and categorized into constriction size distribution criteria and capillary tube model. These criteria depend mainly on particle size, particle morphology, density, pore size, and pore size distribution (Kezdi 1979; Kovacs 1981; Vafai 1996; Maroof et al. 2021b, a).

When fine particles are transported to the void network formed by a coarser skeleton, grains smaller than the controlling constriction size are likely to be transported (Liang et al. 2017). Thus, the eroded fine grains are controlled by the pore geometry. Numerous network models emphasizing fine-grain transport mechanisms through soil pores can be classified as analytical models, constriction-based criteria, and capillary tube model. The former one is discussed in the next section ("Capillary tube models").

Analytical and numerical models

The more simple description for the void space in granular materials consists of envisioning it as a set of larger void spheres (pores) linked by throats (tubes) representing pore constrictions (Schuler 1996). Any movement of fine particles within this network is controlled by the constriction sizes and their occurrence in the material (Khilar and Fogler 1998).

Different analytical models were proposed to compute the constriction size distribution. They are all based on a proposal by Silveira (1965) to simplify the complex configurations giving rise to the constrictions by a set of geometrical configurations (Silveira 1965).

There also exist numerical approaches to the problem based on a numerical representation of the granular material. They are processed on the basis of an image of an actual sample obtained by CT-scan (Dong and Blunt 2009; Homberg et al. 2012; Taylor et al. 2016) after segmentation of the pore space. Finally, the CSD can also be obtained for numerical samples built through the discrete element method (DEM) (Reboul et al. 2008; Taylor et al. 2015; Shire et al. 2016; Seblany et al. 2018; Nguyen et al. 2021). Approaches developed based on CT-scan are specifically powerful since they can address any sample composed of particles with irregular shapes with very different sphericities, angularities, or flatness. However, they always need robust post-processing in order to remove artificial entities created by the very discrete nature of the images (set of voxels) (e.g., (Taylor et al. 2016)).

Controlling constriction size

Pore throats control the particle transport mechanism in porous media due to geometrical restrictions and constriction sizes along flow paths. Studies carried out by Kenney et al. (1985) over a wide range of gradations exhibited that the CSDs, for a given compaction, organized a narrow band of similarly shaped curves when normalized by a representative filter thickness (D_5 or D_{15}). Therefore, smaller filter particles seem to govern the process of filtration. It was also found by Sherard et al. (1984) and Foster and Fell (2001) and is underlying the filter retention criterion of Terzaghi (Terzaghi et al. 1996). Kenney et al. (1985) revealed the concept of controlling constriction size d_c, where this quantity is related to the maximum particle size that can pass through a pore network. Base particles smaller than d_c^* can pass through the granular filter depending on the seepage conditions. The controlling constriction size has a close relationship with the concept of effective opening size that a fine particle will find on any pathway by Witt (1993). More practically, in all these definitions, the granular filter is associated to a mechanical sieve with an equivalent opening size. Indraratna et al. (2007) found that the controlling constriction size (or equivalent opening size) is close to d_c^{35} (constriction diameter that is 35% smaller than the cumulative CSD). Seblany et al. (2021) demonstrated that this quantity can be associted to the largest mode of the CSD, the most represented size in the pore network. Some relationships proposed by researchers are shown in Table 1.

Due to an over-idealization of the soil skeleton, the proposed analytical technique that anticipates the full distribution of constriction sizes using incircling circles to approximate constriction sizes is often found to poorly estimate the CSD for broadly distributed grading (Shire and O'Sullivan 2016). Furthermore, analytical methods may have specific limitations such as gradation or density. Even if Wu et al. (2012) showed that the analytical CSD (Indraratna et al. 2007; Seblany et al. 2021) mainly developed for spherical materials can be used for granular materials with shapes associated that are not perfectly spherical and smooth, they are not adapted to materials with elongated shapes (see also Taylor et al. 2018). In that case, there are more numerous smaller constrictions and larger constrictions sizes than predicted by these formulas. Moreover, angular and elongated particles tend to have smaller mean pore lengths and an increase in tortuosity, leading to a higher probability of clogging of fine particles than granular filters composed of smooth and spherical-like ones (Maroof et al. 2021a; Deng et al. 2023).

There are more precise grain packings and porous skeletons such as the imprint of pore networks (e.g., Vincens

Table 1 Proposed relationship for controlling constriction size

Reference	Relationship		Notation
Kenney et al. (1985)	$d_c^* = 0.25D_5 and d_c^* = 0.20D_{15}$	(1)	
Witt (1993)	$d_p^* = 0.23D_G$	(2)	where D_G is the mean grain size by number (ranging from D_5 to D_{10} and from D_{10} to D_{30} for uniform PSD (Cu < 3))
Sherard et al. (1984)	Max $d_c^* = 0.18D_{15}$	(3)	$d_c^* = 0.09D_{15} to 0.18D_{15}$
Foster and Fell (2001)	Median $d_c^* = 0.16D_{15}$	(4)	$d_c^* = 0.15D_{15} to 0.20D_{15}$
Indraratna et al. (2007)	$d_c^* = d_c^{35}$	(5)	
Seblany et al. (2021)	$d_c^*(e) = d_{cmin} + \frac{e}{e_{max}}\left(d_{OS,L} - d_{cmin}\right)$	(6)	$d_{OS,L} \approx 0.23D_{50SA}$ for continuum grading $d_{OS,L} \approx 0.23D_{55SA}$ for gap-graded material $d_{cmin} \approx \frac{D_0}{6.5}$

et al. 2015; Maroof et al. 2022a), CT-scan and DEM-based models (Taylor et al. 2015), and pore network models (e.g., Daneshian et al. 2021; Veiskarami et al. 2023). Yet, some particular requirements and specific limitations of these methods (Vincens et al. 2015), and the complexity of the real porous skeleton which can be altered for different soils and even in one soil from pore to pore, make them difficult to utilize in practical applications. The use of capillary tube models may address the limitations of these models while taking into account grading, density, and particle shape.

In previous works, the problem of the void size distribution (Sjah and Vincens 2013; Vincens et al. 2015; Seblany et al. 2018, 2021; Maroof et al. 2022a), particle shape classification (Maroof et al. 2020b), the determination of shape coefficients (Maroof et al. 2020a), and the effect of particle morphology on internal instability (Maroof et al. 2021a) have been investigated. These studies showed that sphericity, roundness, and surface texture affect the susceptibility to suffusion, and spherical rounded particles with smooth surfaces are more prone to internal instability and volume change during suffusion. The concept of the capillary tube model developed by Kovacs (1981) is revisited and extended to characterize the pore network and the susceptibility to internal erosion in order to take into account the influence of grading, density, and particle shape of the granular material. This study improved the Kovacs model that integrates the accurate shape coefficient of particles, and it has been validated through previous research and the new experimental data.

Capillary tube models

Kovacs (1981) characterized the average pore size of the coarser fraction directly in terms of the average pipe diameter of a bundle of capillary tubes (Fig. 1). In this definition, the pore size actually denotes the mean size of the throat linking two adjacent pores (Schuler 1996). Afterward, to evaluate the potential movement of finer loss particles, this characteristic size related to a hydraulic process is compared with the mean opening size of the coarser skeleton.

This model takes into account the porosity and mean particle shape of the coarser fraction and indirectly the grain size distribution by expanding its effective diameter rather than computing the direct geometric property of the pore space (controlling constriction size).

Effective diameter

The effective or equivalent mean diameter of a particle, D_{eff}, in a granular medium, is often characterized as the diameter of the smallest circumscribed sphere (D) (Maroof et al. 2020a). In the two-dimensional state, it is defined as the diameter of the encircling circle on the projection plan or the main section of the particle (Kovacs 1981) (Fig. 2).

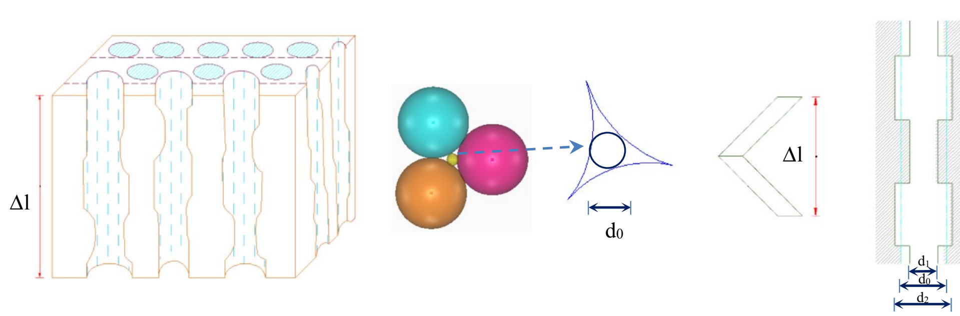

Fig. 1 Bundle of capillary tubes and void size (after Kovacs 1981 and Vafai 1996)

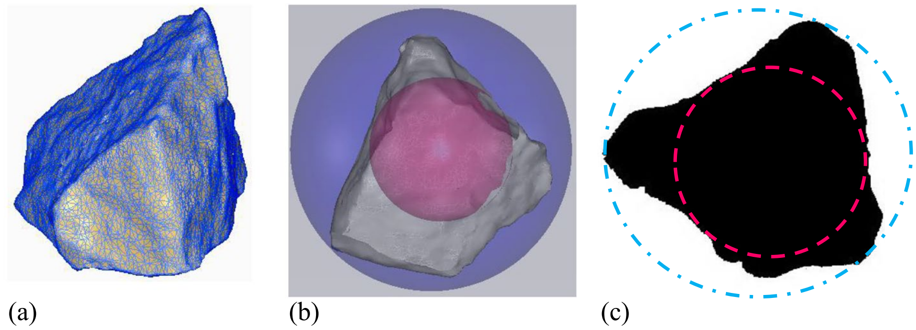

Fig. 2 **a** 3D-reconstructed particle, **b** the smallest circumscribed sphere and largest inscribed sphere, **c** particle projected plan, smallest circumscribed circle, and largest inscribed circle

For grain assemblies with randomly mixed particles, the effective particle diameter can be associated with the equivalent diameter of a mono-size mixture with an identical specific surface area as the heterogeneous mixture (Aubertin et al. 2003). The effective particle diameter is then computed on the basis of the particle size distribution (PSD). The PSD is split into classes with frontiers corresponding to different sieves of different opening sizes.

Knowing the mean particle size $D_{av,i}$ of a given class i, the effective diameter is determined by (Kozeny 1927; Fair and Hatch 1933; Carman 1937; Loudon 1952; Kovacs 1981; Sperry and Peirce 1995; Dolzyk and Chmielewska 2014; Zheng and Tannant 2017):

$$\mathrm{D_{eff}} = \frac{100}{\sum\left({}^{\mathrm{fi}}\!/_{\mathrm{D_{av,i}}} \right)} \; \textit{and} \; \mathrm{D_{av,i}} = \sqrt{\mathrm{D_{li}}\times\mathrm{D_{si}}} \tag{7}$$

where D_{av} is the average grain size of class i, D_{li} and D_{si} are the limits of class i, that is to say, the maximum and minimum particle size (adjacent sieve opening sizes) respectively, and f_i is the grains percentile (mass) of class i. More recently, on the assumption that in a given class i, grains are log-linearly distributed, Carrier (2003) and Zheng and Tannant (2017) proposed to compute $d_{av,i}$ by the relationship:

$$D_{\mathrm{av,i}} = \mathrm{D}_{li}^{b}\mathrm{D}_{si}^{1-b} \tag{8}$$

where b was proposed to be equal to 0.404 for all graded grain sizes (Carrier 2003), 0.68 for poorly graded particles, and 0.90 for gap-graded particle sizes (Zheng and Tannant 2017).

Coarser fraction

In the capillary tube model, the soil is assumed to be composed of two fractions, a finer and a coarser, where fine loose grains can pass through the void formed by the coarser primary fabric (references). Then, PSD is split into a coarser and finer fraction (f) at a given delimitation diameter (D) (Kezdi 1979; Aberg 1992; Li and Fannin 2013; Dallo and Wang 2016).

This latter is supposed to coincide with the point of inflection or $(H/F)_{min}$ for a broadly distributed gradation and the maximum location of the gap in gap-graded soils (Li and Fannin 2013). The value of D_0/D_{85}^{f} at $(H/F)_{min}$, or the end of the gap in gap-graded soils, is very close to $(D_0/D_{85}^{f})_{\max}$ (Li and Fannin 2013). Afterward, the coarser fabric void ratio can be expressed in terms of e and f (Kezdi 1979):

$$e_c = \frac{e+f}{1-f} \tag{9}$$

Furthermore, the porosity of the coarser fraction is assumed:

$$n_c = n + f(1-n) \tag{10}$$

A threshold of about 35% separates possible loose finer fraction particles from fixed coarse grains. Meanwhile, more fine particles caused floating coarser particles in the matrix of fines (Skempton and Brogan 1994).

Shape factor and specific surface area

Surface roughness and specific surface area of particles (SSA, S_0) are key information that can explain phenomena at the microscale (Maroof et al. 2020a). An ideal sphere or cube has the lowest value for SSA defined as the ratio between the surface area and the volume ratio or mass (Chapuis 2012):

$$SSA = \frac{6}{D} \tag{11}$$

where D denotes the side of a cube or the diameter of a sphere. The SSA of a heterogeneous sample containing irregular particle shapes can be defined as (Heywood 1933; Carman 1939; Loudon 1952; Kovacs 1981):

$$\mathrm{SSA} = \alpha\Big(\sum_{i=1}^{n} \mathrm{x}_i \mathrm{S}_i\Big) = 6\sum_{i=1}^{n} {}^{\mathrm{x}_i}\!/_{\alpha_i D_{xi}} \tag{12}$$

where α_i and x_i denote the mean shape factor and weight percentile of particles in the ith class of the gradation curve,

D_{xi} and S_i are the average size and surface area of equivalent spheres in the ith class, respectively.

Indeed, the SSA of particles is controlled by the grain size and shape. As a result, it is defined as the ratio of the shape factor to the effective particle diameter (Kovacs 1981; Maroof et al. 2020a):

$$\frac{\mathrm{A}}{\mathrm{V}} = \frac{\pi}{\mathrm{D_{eff}}} \tag{13}$$

Shape factor, α, is a dimensionless coefficient that is only dependent on the shape of the grain which illustrates the differences between actual nonspherical grains and ideal smooth spheres (Fair and Hatch 1933; Loudon 1952; Hunger and Brouwers 2009). Kovacs proposed different values for the shape factor of grains including spheroid, rounded, angular, and laminated grains equal to 6, 7–9, 9–11, and 20, respectively (Kovacs 1981).

Moreover, the shape factor has a strong connection to the particle sphericity, roundness, and roughness and thus to particle shape indicators. Numerous shape coefficients were obtained using various sphericity definitions, such as Wadell's true sphericity (ψ_s) and the inscribed-circumference sphere ratio (see Fig. 2) (ψ_{ic}) (Wadell 1933; Maroof et al. 2020b).

The surface texture of the particle, as well as sphericity and roundness, can also affect the pore network. Indeed, the possibility of fine particle blockage in the pore throats increases as roughness increases (Maroof et al. 2021a). Relationships for particle shape factors with different sphericities, rough textures, and smooth surfaces were proposed by Maroof et al. (2020a) (Eqs. 13 and 14). The shape factor of particles with different forms is accounted for in the new model (Eqs. 15 and 17 to 21).

$$\alpha = 6.3\psi_{ic}^{-0.85} \quad \text{rough texture} \tag{14}$$

$$\alpha = 6.0\psi_{ic}^{-0.72} \quad \text{smooth surface} \tag{15}$$

Equivalent tube diameter

Due to the complexity of pore network geometry, it is difficult to measure the pore size directly from the grain size distribution (Liang et al. 2017). Within the framework of the capillary tube model, the pore space is modeled as a bundle of straight cylindrical capillary pipes with smooth walls, by an extension of Hagen–Poiseuille law (Carman 1937; Bear 1972).

The surface area to volume of the pores is equal to the ratio of the wetted surface or particle surface (A) to the volume of the conduit (V_p). As a result, the following equation can be used to define the d_0, d_1, and d_2 (see Fig. 1) (Kovacs 1981):

$$\frac{\pi_0 \Delta l}{\frac{\pi}{4} d_0^2 \Delta l} = \frac{\mathrm{A}}{\mathrm{V_p}} = \frac{\mathrm{A}}{\frac{\mathrm{nV}}{1-\mathrm{n}}} = \frac{1-\mathrm{n}}{\mathrm{n}}\frac{\mathrm{A}}{\mathrm{V}} = \frac{1-\mathrm{n}}{\mathrm{n}}\frac{a}{\mathrm{D_{eff}}}, \text{ then } d_0 = 4\frac{n}{1-n}\frac{D_{eff}}{\alpha} \tag{16}$$

and

$$d_1 = 0.67d_0, d_2 = 1.25d_0 \tag{17}$$

where V is the volume of the sample, Δl is the length of the conduit, and d_1 and d_2 denote the minimum and maximum diameter of the pore channel (see Fig. 1), respectively.

The mean capillary tube diameter is determined by Eq. 15, and it is the basis of the capillary tube model as discussed in the next section.

Proposed capillary tube model

In the capillary tube model, the probability of fine particle movement and suffusion potential is assessed by comparing the smallest pore diameter (d_1) or the mean diameter of the pores between the coarser fabric (d_0) when the arching effect and inhomogeneity are considered and the minimum particle diameter (D_{min} or D^f_{85}) (Kovacs 1981; Kenney et al. 1985; Aberg 1993; Wan and Fell 2008). Some researchers, modifying the Kovacs model, suggested substituting the average pore diameter of the coarser part by the controlling constriction size of the coarser fraction (Li and Fannin 2013; Dallo and Wang 2016)).

Kovacs (1981) criterion considers the influence of particle shape with the shape factor (α). It means that an increase in grain angularity results in an increase in the shape coefficient (Maroof et al. 2020a) and a decrease in the mean diameter of pores. The shape of soil grains also influences the sample porosity (Maroof et al. 2022b) which is also taken into account in the capillary tube model. Table 2 illustrates the proposed capillary tube model and shape coefficient for predicting the suffusion potential.

Developed capillary tube model

Experimental work

In this study, proposed Kenney and Lau's (1985, 1986) boundaries between internally stable and unstable soils were examined. Therefore, the internal stability of two ideal particle size distribution curves was evaluated; the Fuller and Thomson (Fuller and Thomson 1907) and the Lubochkov PSD curves (Lubochkov 1969). These new results were utilized both for developing the new model and for comparison with other geometrical criteria.

Table 2 Proposed capillary tube model and shape coefficient

Reference	Formula		Particle shape	Shape coefficient (α, SF)	Definition
Kovacs, (Kovacs 1981)	$d_0 = 4.0\frac{n_c}{1-n_c}\frac{D^c_{eff}}{\alpha} \le D_{min}$ *or* $d_1 = 2.7\frac{n_c}{1-n_c}\frac{D^c_{eff}}{\alpha} \le D_{min}$ *and* $D_{min} = D^f_{85}$		Spheroid	6	d_1: smallest pores diameter d_0: mean pore size $d_{cont.}$: controlling constriction size, (Kenney et al. 1985)
		(18)	Subrounded	7–9	D^f_{85}: particle diameter 85th percent in the finer fraction
			Angular	9–11	D^c_{eff} and n_c effective diameter and porosity of the coarser fraction, respectively
		(19)	laminated	20	
Li and Fannin, (Li and Fannin 2013)	$d_0 = 4.0\frac{n_c}{1-n_c}\frac{D^c_{eff}}{\alpha}$ *and* $D_{min} = 2.3D^f_{85}$	(20)	Rounded	6	
			Angular	8	
Dallo and Wang, (Dallo and Wang 2016)	$d_0 = 4.0\frac{n_c}{1-n_c}\frac{D^c_{eff}}{\alpha}$ *and* $D_{min}=2.75D^f_{85}$ *or* $d_{cont.} = d_0/2.75$	(21)	Rounded	6	
			Angular	8	
Current study	$d_0 = 4.0\frac{n_c}{1-n_c}\frac{D^c_{eff}}{\alpha}$ $D_{margin} = 2.3D^f_{85}$, *and* $D_{min} = 2.8D^f_{85}$		Rough glass bead	6.3	
			Rounded	7.2	
		(22)	Crushed	9	
			Flat	13	
			Elongated*	24	

*Shape coefficient of particles with different forms can be determined by Eqs. 14 and 15

Fuller and Thomson (1907) depict an ideal gradation for an optimum density represented by:

$$F_d = (d/d_{100})^m \tag{23}$$

if $m = 0.5$ since mass increment $H = F_{4d} - F_d = F((4)^{0.5} - 1) = 1.0F$

Lubochkov (1969) proposed that suffusion susceptibility depends on the particle size distribution shape and proposed upper and lower boundary curves for internally stable soils (Kovacs 1981), with lower limit (Kenney and Lau 1985):

$$F_d = 0.6(d_x/d_{60})^{0.6} \tag{24}$$

and $H = 1.297$F. Kenney and Lau (1985) amended the Lubochkov lower limit to yield a limiting PSD curve $H = 1.3$F. Comments in the literature (Milligan 1986; Sherard and Dunnigan 1986) and the further test data resulted in the subsequently revised threshold consistent with Fuller and Thompson's (1907) boundary to $(H/F)_{min} \le 1.0$ (Kenney and Lau 1986).

The previous experimental results show that the Lubochkov lower limit curve is a stable grading (Kenney and Lau 1985). Furthermore, Fuller gradation is also internally stable (Kenney and Lau 1986; Milligan 1986; Li 2008). Particle shape, whole PSD curve, and sample density have been neglected by many geometrical criteria of internal stability assessment. Obviously, constriction sizes reduce as relative densities increase. The Fuller gradation is partially internally stable at higher compaction levels ($R_d \ge 70\%$) (Indraratna et al. 2015).

Herein, the effect of particle shape on internal stability was evaluated by creating samples where each of them has grains with similar shapes. SSA and shape coefficient for the studied mixtures were evaluated using the analytical formula. The average shape factor for rounded, angular, flat, and elongated particles is 7.2, 9.3, 14, and 23, respectively (Maroof et al. 2020a).

Ten experimental tests were performed in a medium-dense condition (relative density equal to $50 \pm 8\%$). These tests were conducted on Well-graded soils that are similar to the ideal Fuller and Lubochkov PSD curves, with five distinct particle shapes including spherical glass beads, rounded, angular, flaky, and elongated grains. The grading, particle shape, and particle packing properties of the test materials are depicted in Tables 3.

The experimental results showed that the samples with spherical and medium sphericity/rounded grains were classified as internally unstable, and specimens containing elongated particles were categorized as internally stable, both in Fuller and Lubochkov curves (more details about internal instability occurrence have been elucidated in the Maroof et al. 2021a). The specimen with angular grain in the

Table 3 General properties of the test materials

PSD	USCS classification[a]	d_{50} (mm)	Cu	Cc	Particle shape	α	e_{max}[b]	e_{min}[c]	e
Fuller	SW-SM	2.52	36.7	2.36	Spherical	6.0	0.35	0.19	0.27
					Rounded	7.2	0.48	0.21	0.35
					Crushed	9.3	0.59	0.28	0.41
					Flat	14.0	0.66	0.34	0.52
					Elongated	23.0	0.93	0.56	0.78
Lubochkov	SW-SM	2.94	20.4	2.11	Spherical	6.0	0.37	0.22	0.30
					Rounded	7.2	0.49	0.28	0.39
					Crushed	9.3	0.61	0.32	0.44
					Flat	14.0	0.70	0.35	0.53
					Elongated	23.0	1.16	0.70	0.89

[a]ASTM D2487 (2017)
[b]ASTM D4253-00 (2006)
[c]ASTM D4254-00 (2006)

Lubochkov curve is categorized as transient, and the sample having flaky particles is internally unstable. Furthermore, in the Fuller curve, samples with angular and flaky particles are categorized as samples with internal stability (see Table 5). These findings agree with previous experimental work that spherical/rounded particles are more likely to suffusion (Slangen and Fannin 2017; Hassani 2020; Maroof et al. 2021b, a). Meanwhile, this change in particle form makes them easier to pack and causes lower void ratios (see Table 3 and Maroof et al. 2022b).

Exploring new data

The capillary tube model considers both density and shape as well as particle size. In these methods, particle geometry is characterized based on roundness and sphericity (Kovacs 1981) or roundness (Chang and Zhang 2013; Li and Fannin 2013), and the shape coefficient was estimated by visual comparison. The boundary thresholds proposed by Li and Fannin and Dallo and Wang were established using a database compiling soils and glass bead specimens. In their work, soil samples were assumed to have a shape coefficient of 8 (sub-angular to angular soils) (Li 2008; Li and Fannin 2013; Dallo and Wang 2016).

Maroof et al. (2021a, b) performed 26 suffusion tests on five different gradations and six various shapes. According to Kovacs capillary tube model, the average pore diameter (Eq. 15) and D^f_{85} of the finer fraction were determined. Summary results for the capillary tube model are presented in Table 4.

Modified capillary tube model

Aside from the binary stable-unstable qualification for the granular material, safety margins are defined to involve uncertainties in the engineering design process. These two boundaries are defined as $d_0 = 1.5D^f_{85}$ and $d_0 = D^f_{85}$ for the upper and lower side, respectively (Li and Fannin 2013; Dallo and Wang 2016).

The different prediction in the Kovacs criterion is due to several factors: the variation of the cross-sectional area of the conduit, the tortuosity of the mean hydraulic tube, and the pore interconnectivity (Chatzis and Dullien 1977; Khilar and Fogler 1998; Li 2008).

Li and Fannin (2013) suggested a boundary threshold for a database of 42 suffusion tests ($d_0 = 2.3D^f_{85}$) (Li and Fannin 2013); Nevertheless, Dallo and Wang (2016) proposed a boundary threshold to modify this value to $d_0 = 2.75D^f_{85}$ after analyzing a database of 32 tests where the prediction of Kovacs model resulted wrong in four cases among 32. So, the actual threshold margin will need to be adjusted. Exploring suffusion tests performed by Maroof et al. (2021b) and new experimental tests, the upper boundary was shifted to $d_0 = 2.8D^f_{85}$ d_0= $2.8D^f_{85}$. The d_0= $2.3D^f_{85}$ is a margin for internal stable soils, and the zone between $d_0 = 2.3D^f_{85}$ and $d_0 = 2.8D^f_{85}$ is specified as the transient zone. The flowchart assessing the modified model is depicted in Fig. 3. This model incorporates the effective grain size distribution and porosity to the mean pore size, through specific surface area, and the shape factor.

The results are given in Fig. 4 and Table 5, including the results derived from experiments performed by Maroof et al. (2021b) and current experiments. The transient zone was suggested because besides the parameters considered in capillary tube models, other factors such as hydrodynamical conditions (hydraulic gradient and seepage flow) and stress conditions (Zhang et al. 2023) also affect internal stability/instability which is usually ignored in geometrical criteria.

Table 4 Summary of the relevant results for the capillary tube model

PSD	Particle shape	f	e	n_c	D^C_{eff}	α	D^f_{85}	d_0	d_0/D^f_{85}
K	Glass Bead	0.20	0.45	0.45	3.65	6.0	1.90	1.98	1.04
K	Rounded	0.20	0.49	0.46	3.65	7.2	1.90	1.75	0.92
K	Crushed	0.20	0.66	0.52	3.65	9.3	1.90	1.69	0.89
K	Flat	0.20	0.73	0.54	3.65	14.0	1.90	1.21	0.63
K	Elongated	0.20	1.08	0.62	3.65	23.0	1.90	1.02	0.53
B	Glass bead	0.12	0.39	0.37	2.86	6.0	0.31	1.11	3.56
B	Rough glass bead	0.12	0.43	0.38	2.86	6.5	0.31	1.09	3.52
B	Rounded	0.12	0.44	0.39	2.86	7.2	0.31	1.01	3.26
B	Crushed	0.12	0.59	0.45	2.86	9.3	0.31	0.99	3.20
B	Flat	0.12	0.67	0.47	2.86	14.0	0.31	0.73	2.37
B	Elongated	0.12	1.06	0.57	2.86	23.0	0.31	0.67	2.15
M1	Glass bead	0.14	0.37	0.37	2.74	6.0	0.20	1.09	5.43
M1	Rounded	0.14	0.42	0.39	2.74	7.2	0.20	0.99	4.96
M1	Crushed	0.14	0.58	0.46	2.74	9.3	0.20	0.99	4.93
M1	Flat	0.14	0.68	0.49	2.74	14.0	0.20	0.75	3.73
M1	Elongated	0.14	1.03	0.58	2.74	23.0	0.20	0.65	3.24
GP-1	Glass bead	0.15	0.44	0.41	3.07	6.0	0.28	1.42	5.06
GP-1	Rounded	0.15	0.51	0.44	3.07	7.2	0.28	1.32	4.73
GP-1	Crushed	0.15	0.64	0.48	3.07	9.3	0.28	1.23	4.38
GP-1	Flat	0.15	0.76	0.52	3.07	14.0	0.28	0.94	3.35
GP-1	Elongated	0.15	1.09	0.59	3.07	23.0	0.28	0.78	2.78
G13	Glass bead	0.15	0.42	0.40	3.36	6.0	0.19	1.50	7.91
G13	Rounded	0.15	0.46	0.42	3.36	7.2	0.19	1.35	7.10
G13	Crushed	0.15	0.68	0.49	3.36	9.3	0.19	1.41	7.43
G13	Flat	0.15	0.75	0.52	3.36	14.0	0.19	1.02	5.38
G13	Elongated	0.15	1.03	0.58	3.36	23.0	0.19	0.81	4.27
Lu	Glass bead	0.13	0.30	0.33	1.74	6.0	0.16	0.57	3.54
Lu	Rounded	0.13	0.39	0.37	1.74	7.2	0.16	0.57	3.58
Lu	Crushed	0.13	0.44	0.40	1.74	9.3	0.16	0.49	3.09
Lu	Flat	0.13	0.53	0.43	1.74	14.0	0.16	0.38	2.36
Lu	Elongated	0.13	0.89	0.54	1.74	23.0	0.16	0.35	2.22
Fu	Glass bead	0.17	0.27	0.35	1.55	6.0	0.18	0.55	3.04
Fu	Rounded	0.17	0.35	0.38	1.55	7.2	0.18	0.53	2.97
Fu	Crushed	0.17	0.41	0.41	1.55	9.3	0.18	0.47	2.59
Fu	Flat	0.17	0.52	0.45	1.55	14.0	0.18	0.37	2.05
Fu	Elongated	0.17	0.78	0.53	1.55	23.0	0.18	0.32	1.77

Verification of the model

The most common geometrical criteria are a function of particle size distribution depending on the shape or slope of the PSD curve (Kezdi 1979; Kenney and Lau 1985; Li and Fannin 2008; Chang and Zhang 2013; Chapuis 2021). In addition to grain size distribution, it is necessary to take into account other factors such as particle shape and density for internal instability assessment.

The current and previous experimental works exhibited that soils with different grain shapes have various levels of internal stability/instability. The angular/low sphericity particles with rough textures are more resistant to suffusion, and these criteria are more conservative for grains with low sphericity, angular particles, or particles with a rough texture (Maroof et al. 2021a). These results showed that soils with the same grain size distribution but different particle shapes exhibit different levels of suffusion susceptibility. As a result, when common geometrical criteria are applied to soil samples with various grain shapes and densities, they have inaccurate predictions.

Previous databases of soil and glass bead samples are presented in Li (2008), Li and Fannin (2013), and Dallo and Wang (2016). Summary results of new and past laboratory permeameter tests (Hassani 2020; Maroof et al. 2021a) and internal instability assessment using proposed

Table 5 Summary results of permeameter tests and internal instability assessment using proposed criteria and developed capillary tube mode

PSD	Soil ID	Kezdi (1979)	Kenny and Lau (1986)	Burenkova (1993)	Wan and Fell (2008)	Chang and Zhang (2013)	Li and Fannin (2013)[d]	Developed Kovacs model	Experimental result[a]
K	*GB*	*S*	*S*	*S*	*T*	*S*	*S*	*S*	*S*
	R						*S*	*S*	*S*
	C						*S*	*S*	*S*
	F						*S*	*S*	*S*
	E						*S*	*S*	*S*
B	*GB*	*S*	T^b	*U*	*T*	*T*	*U*	*U*	*U*
	GB-Ro						*U*	*U*	*T*
	R						*U*	*U*	*U*
	C						*U*	*U*	*S*
	F						*U*	*T*	*T*
	E						*S*	*T*	*S*
M1	*GB*	*U*	*U*	*U*	*U*	*U*	*U*	*U*	*U*
	R						*U*	*U*	*U*
	C						*U*	*U*	*U*
	F						*U*	*U*	*U*
	E						*U*	*U*	*T*
GP-1	*GB*	*U*	*U*	*U*	*T*	*U*	*U*	*U*	*U*
	R						*U*	*U*	*U*
	C						*U*	*U*	*U*
	F						*U*	*U*	*U*
	E						*U*	*T*	*T*
G3-13	*GB*	*U*	*U*	*U*	*U*	*U*	*U*	*U*	*U*
	R						*U*	*U*	*U*
	C						*U*	*U*	*U*
	F						*U*	*U*	*U*
	E						*U*	*U*	*U*
Lu	*GB*	*U*	U^c	*S*	*T*	*U*	*U*	*U*	*U*
	R						*U*	*U*	*U*
	C						*U*	*U*	*T*
	F						*U*	*T*	*U*
	E						*S*	*S*	*S*
Fu	*GB*	*U*	T^b	*S*	*S*	*T*	*U*	*U*	*U*
	R						*U*	*U*	*U*
	C						*U*	*T*	*S*
	F						*S*	*S*	*S*
	E						*S*	*S*	*S*

S stable, *U* unstable, *T* transient, *GB* glass bead, *R* rounded particle, *C* crushed aggregate (angular), *F* flat (slate), *E* elongated (weathered pyramid basalt).

[a]Data From Maroof et al. (2021a, b) and the current study.

[b]$(H/F)_{min} = 1.0$

[c]$(H/F)_{min} = 1.3$

[d]The results were determined by employing the precise shape factor with the Li and Fannin model.

criteria and improved capillary tube model are revealed in Table 5.

In this model, particle shape was considered with the shape coefficient. By employing an appropriate shape factor, this model estimates the internal instability of soil with reasonable accuracy. Li and Fannin and Dallo and Wang assumed soil samples sub-angular to angular soils (shape factor = 8); by employing precise shape factor with the Li and Fannin boundary, the results of the internal stability were assessed (Table 5).

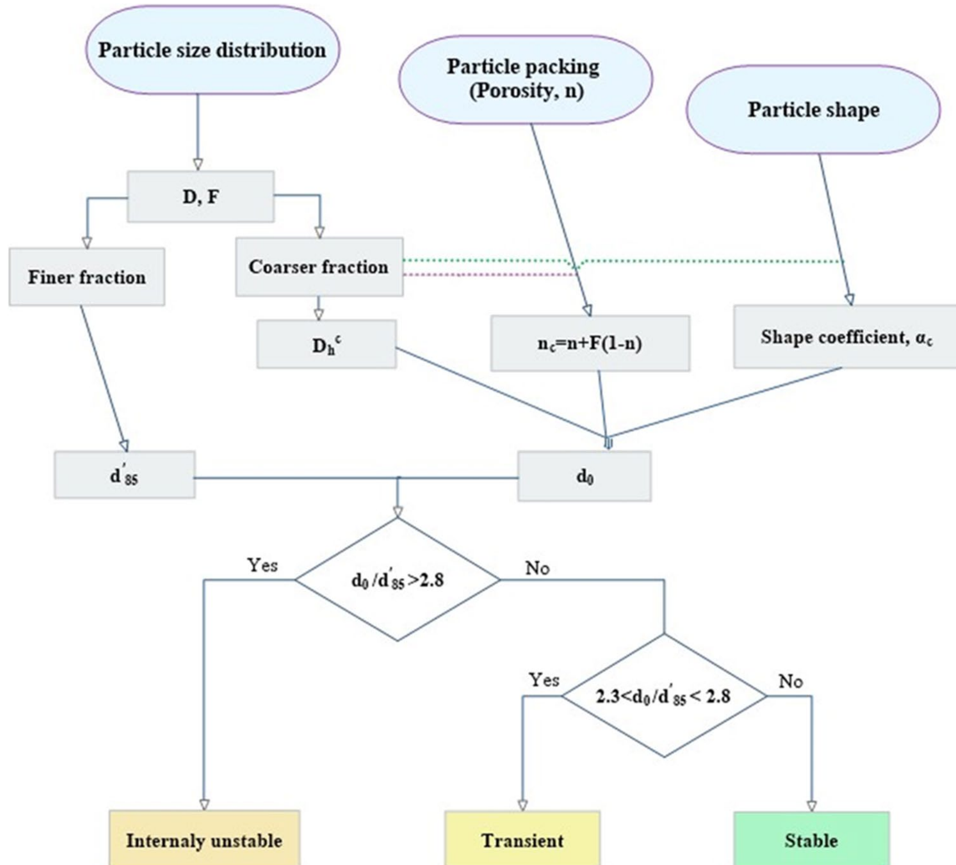

Fig. 3 The flowchart assessing the modified capillary tube model

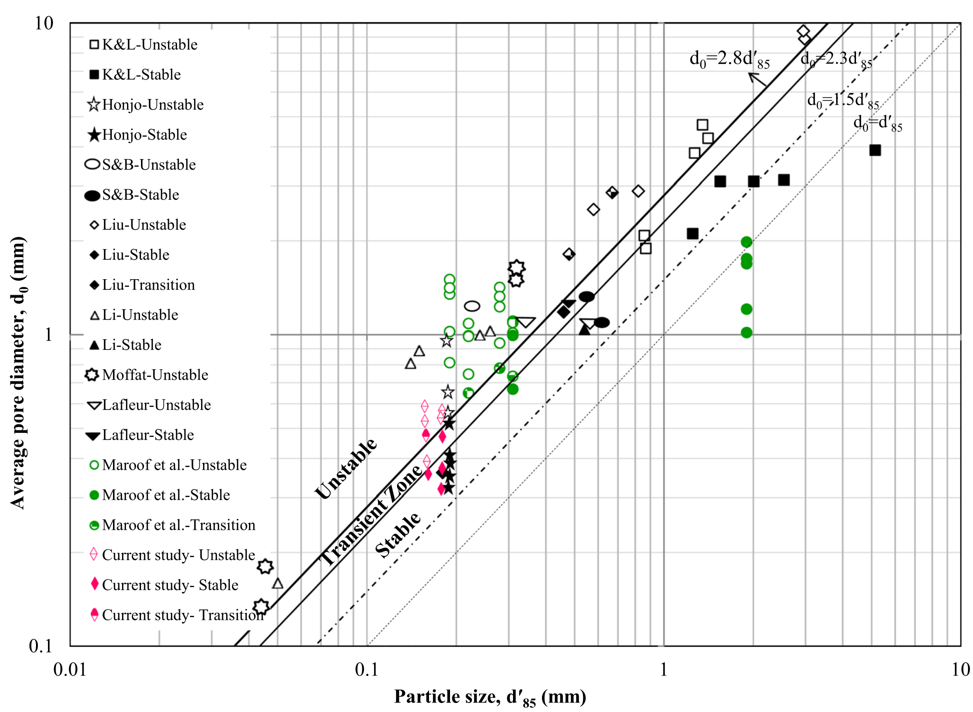

Fig. 4 The proposed and modified boundary threshold of the capillary tube model

This correlation is developed by considering the porosity and grain shape in the formulation of the capillary tube model. Nevertheless, this model originally connects the SSA of the particles with the SSA of a capillary tube and compares its pores with the size of the loose fine grains. The constrictions have a surface in common with the passed grains, when two or more particles enter a pore where the cross-section of the pores is much more than that of a throat. Therefore, modeling distributions of both constriction and pores with a bundle of capillary tubes is more simplified as compared to realistic models. This modified model solved this problem by moving the boundaries of the Kovacs model. Nevertheless, other factors such as porosity variation, hydrodynamic conditions, fluid properties, and applied stress changed pore constriction and particle transport, and the transient zone enables consideration of them by more detailed experimental investigation.

Conclusions

The boundary between internal stable and unstable soils can be conveyed by pore diameter and loose fine particle comparison. The capillary tube model considers particle shape and porosity as well as particle gradation and may be favored in engineering practice. By the way, this model has been rarely validated based on experimental data, and it has not been commonly used.

In the current study, using the previous database of 42 permeameter tests, exploring new data, including 26 data, the validity of the proposed capillary tube models was examined. Furthermore, 10 new suffusion tests with different particle shapes, on the boundary threshold of Kenny and Lau's criteria, were performed.

The experimental test showed that as particle sphericity, roundness, and smoothness increase, the particle migration in the coarser skeleton facilitates and promotes the internal instability of the soil matrix.

Additionally, based on experimental data, the capillary tube model was developed and enhanced for practical applications. New margins to internal instability have been established as $d_0 = 2.3d^f_{85}$ and $d_0 = 2.8d^f_{85}$. These threshold boundaries classified soil samples as internally stable, transient zone, or unstable.

The proposed boundaries were found to be reasonably accurate when compared to experimental results. A few wrong predictions were fixed in the safe boundaries, while only one internally unstable soil was predicted to be internally stable.

Notation PSD/GSD: Particle/grain size distribution; D_x, d_x: Grain size that *X* percent is finer than it; *D*: Particle size (mm); D_{avg} : Average grain size of the PSD curve; *f*: Finer fraction; f_i: Percentage of grains that are finer from *i* or at *i* fragment; *n*: Porosity; *SSA* or S_0 : Specific surface area in $1/m$ or m^2/g; α, *SF*: Shape factor, shape coefficient; D_{eff}, $\mathrm{D_h}$: Effective grain size; d_2 : Maximum pores diameter; φ_{ic} : Inscribed-circumscribed sphere ratio; CSD: Constriction size distribution; *F*, F_d: Percentage finer than *D*, mass passing; *H*: Mass fraction between diameter *D* and 4*D*, mass increment; D_i : The size of the grain that *i* percent is finer; $\mathrm{D_{85}\prime}$,$\mathrm{D^f_{85}}$: Grain size commensurate 85% in the finer fraction; n_c : Porosity of the coarser fraction; $\mathrm{d}_{cont.}$: Controlling constriction size; R_d: Relative density; D^C_{eff}, D^C_h : Effective particle diameter of the coarser fraction; d_1 : Minimum pore diameter; d_0 : Mean pores diameter; φ_s : True sphericity

Acknowledgements The authors truthfully appreciate the anonymous reviewers for their valuable comments and suggestions.

Data Availability The data that support the findings of this study are available from the corresponding author, upon reasonable request.

References

Aberg B (1992) Void ratio of noncohesive soils and similar materials. ASCE J Geotech Eng 118:1315–1334

Aberg B (1993) Washout of grains from filtered sand and gravel materials. J Geotech Eng 119:36–53. https://doi.org/10.1061/(ASCE)0733-9410(1993)119:1(36)

ASTM D2487 (2017) Standard practice for classification of soils for engineering purposes (Unified Soil Classification System). ASTM International, West Conshohocken

ASTM D4253-00 (2006) Standard test methods for maximum index density and unit weight of soils using a vibratory table. ASTM International, West Conshohocken

ASTM D4254-00 (2006) Standard test methods for minimum index density and unit weight of soils and calculation of relative density. ASTM International, West Conshohocken

Aubertin M, Mbonimpa M, Bussière B, Chapuis RP (2003) A model to predict the water retention curve from basic geotechnical properties. Can Geotech J 40:1104–1122. https://doi.org/10.1139/t03-054

Bear J (1972) Dynamics of fluids in porous media. Elsevier, New York

Berkowitz B, Ewing RP (1998) Percolation theory and network modeling applications in soil Physics. Surv Geophys 19:23–72. https://doi.org/10.1023/A:1006590500229

Burenkova VV (1993) Assessment of suffusion in non-cohesive and graded soils. In: Filters in Geotechnical and Hydraulic Engineering. Balkema, Rotterdam, pp 357–360

Carman PC (1937) Fluid flow through granular beds. Chem Eng Res Des 15:S32–S48. https://doi.org/10.1016/S0263-8762(97)80003-2

Carman PC (1939) Permeability of saturated sands, soils and clays. J Agric Sci 29:262–273. https://doi.org/10.1017/S0021859600051789

Carrier WD (2003) Goodbye, Hazen; Hello, Kozeny-Carman. J Geotech Geoenvironmental Eng 129:1054–1056. https://doi.org/10.1061/(ASCE)1090-0241(2003)129:11(1054)

Chang DS, Zhang LM (2013) Extended internal stability criteria for soils under seepage. Soils Found 53:569–583. https://doi.org/10.1016/j.sandf.2013.06.008

Chapuis RP (2012) Predicting the saturated hydraulic conductivity of soils: a review. Bull Eng Geol Environ 71:401–434. https://doi.org/10.1007/s10064-012-0418-7

Chapuis RP (2021) Analyzing grain size distributions with the modal decomposition method: potential for future research in engineering geology. Bull Eng Geol Environ 80:6667–6676. https://doi.org/10.1007/s10064-021-02341-z

Chatzis I, Dullien FAL (1977) Modelling pore structure by 2-D And 3-D networks with applicationto sandstones. J Can Pet Technol 16:97–108. https://doi.org/10.2118/77-01-09
Dallo YAH, Wang Y (2016) Determination of controlling constriction size from capillary tube model for internal stability assessment of granular soils. Soils Found 56:315–320. https://doi.org/10.1016/j.sandf.2016.02.013
Daneshian B, Habibagahi G, Nikooee E (2021) Determination of unsaturated hydraulic conductivity of sandy soils: a new pore network approach. Acta Geotech 16:449–466. https://doi.org/10.1007/s11440-020-01088-3
Deng Z, Chen X, Jin W, Wang G (2023) Effect of gradation characteristics and particle morphology on internal erosion of sandy gravels: a large-scale experimental study. Water 15:2660. https://doi.org/10.3390/w15142660
Dolzyk K, Chmielewska I (2014) Predicting the coefficient of permeability of non-plastic soils. Soil Mech Found Eng 51:213–218. https://doi.org/10.1007/s11204-014-9279-3
Dong H, Blunt MJ (2009) Pore-network extraction from micro-computerized-tomography images. Phys Rev E - Stat Nonlinear, Soft Matter Phys 80:1–11. https://doi.org/10.1103/PhysRevE.80.036307
Fair GM, Hatch LP (1933) Fundamental factors governing the streamline flow of water through sand. J Am Water Works Assoc 25:1551–1565. https://doi.org/10.1002/j.1551-8833.1933.tb18342.x
Fan Z, Hu C, Zhu Q et al (2021) Three-dimensional pore characteristics and permeability properties of calcareous sand with different particle sizes. Bull Eng Geol Environ 80:2659–2670. https://doi.org/10.1007/s10064-020-02078-1
Foster M, Fell R (2001) Assessing embankment dam filters that do not satisfy design criteria. J Geotech Geoenvironmental Eng 127:398–407. https://doi.org/10.1061/(ASCE)1090-0241(2001)127:5(398)
Fuller W, Thomson S (1907) The laws of proportioning concrete. Trans Am Soc Civ Eng 59:67–143. https://doi.org/10.1061/TACEAT.0001979
Hassani M (2020) Effect of particle shape on internal erosion of cohesionless soils. Dissertation, Shahid Beheshti University of Tehran (in Persian)
Heywood H (1933) Calculation of the specific surface of a powder. Proc Inst Mech Eng 125:383–459. https://doi.org/10.1243/PIME_PROC_1933_125_021_02
Homberg U, Baum D, Prohaska S, et al (2012) Automatic extraction and analysis of realistic pore structures from μCT data for pore space characterization of graded soil. In: Proceedings of the 6th International Conference Scour and Erosion (ICSE-6). Paris, pp 66–73
Hunger M, Brouwers HJH (2009) Flow analysis of water-powder mixtures: application to specific surface area and shape factor. Cem Concr Compos 31:39–59. https://doi.org/10.1016/j.cemconcomp.2008.09.010
Indraratna B, Vafai F (1997) Analytical model for particle migration within base soil-filter system. J Geotech Geoenvironmental Eng 123:100–109. https://doi.org/10.1061/(asce)1090-0241(1997)123:2(100)
Indraratna B, Raut AK, Khabbaz H (2007) Constriction-based retention criterion for granular filter design. J Geotech Geoenvironmental Eng 133:266–276. https://doi.org/10.1061/(ASCE)1090-0241(2007)133:3(266)
Indraratna B, Israr J, Rujikiatkamjorn C (2015) Geometrical method for evaluating the internal instability of granular filters based on constriction size distribution. J Geotech Geoenvironmental Eng ASCE 141:1–14. https://doi.org/10.1061/(ASCE)GT.1943-5606.0001343
Istomina V s (1957) Filtration stability of soils. Gostroizdat, Moscow, Leningrad (in Russian)
Kenney TC, Lau D (1985) Internal stability of granular filters. Can Geotech J 22:215–225. https://doi.org/10.1139/t86-068
Kenney TC, Lau D (1986) Internal stability of granular filters: Reply. Can Geotech J 23:420–423. https://doi.org/10.1139/t86-068
Kenney TC, Chahal R, Chiu E et al (1985) Controlling constriction sizes of granular filters. Can Geotech J 22:32–43. https://doi.org/10.1139/t85-005
Kezdi A (1979) Soil physics- selected topics. Elsevier, Amsterdam
Khilar KC, Fogler HS (1998) Migrations of fines in porous media. Springer, Netherlands
Kovacs G (1981) Seepage hydraulics. Elsevier Science, Amsterdam
Kozeny M (1927) Uber kapillare Leitung des Wassers im Boden. Sitzungsber Akad Wiss, Wien 136:271–306
Li M, Fannin RJ (2008) Comparison of two criteria for internal stability of granular soil. Can Geotech J 45:1303–1309. https://doi.org/10.1139/T08-046
Li M, Fannin RJ (2013) Capillary tube model for internal stability of cohesionless soil. J Geotech Geoenvironmental Eng 139:831–834. https://doi.org/10.1061/(ASCE)GT.1943-5606.0000790
Li M (2008) Seepage induced instability in widely graded soils. Dissertation, University of British Columbia
Liang Y, Yeh T-CJ, Zha Y et al (2017) Onset of suffusion in gap-graded soils under upward seepage. Soils Found 57:849–860. https://doi.org/10.1016/j.sandf.2017.08.017
Loudon AG (1952) The computation of permeability from simple soil tests. Géotechnique 3:165–183. https://doi.org/10.1680/geot.1952.3.4.165
Lubochkov (1969) The calculation of suffossion properties of noncohesive soils when using the non-suffossion analog. In: Proceedings of international conference on hydraulic research. Pub Technical University of Brno, Svazek B-5 (in Russian), Brno, Czechoslovakia, pp 135–148
Maroof A, Mahboubi A, Noorzad A (2020a) A new method to determine specific surface area and shape coefficient of a cohesionless granular medium. Adv Powder Technol 31:3038–3049. https://doi.org/10.1016/j.apt.2020.05.028
Maroof A, Mahboubi A, Noorzad A, Safi Y (2020b) A new approach to particle shape classification of granular materials. Transp Geotech 22:100296. https://doi.org/10.1016/j.trgeo.2019.100296
Maroof A, Mahboubi A, Noorzad A (2021a) Effects of grain morphology on suffusion susceptibility of cohesionless soils. Granul Matter 23:8. https://doi.org/10.1007/s10035-020-01075-1
Maroof A, Eidgahee DR, Mahboubi A (2022) Particle morphology effect on the soil pore structure. In: Feng G (ed) Part of the Lecture Notes in Civil Engineering book series (LNCE 213), pp 1–10. Springer Singapore, Singapore
Maroof A, Mahboubi A, Vincens E, Noorzad A (2022b) Effects of particle morphology on the minimum and maximum void ratios of granular materials. Granul Matter 24:41. https://doi.org/10.1007/s10035-021-01189-0
Maroof A, Mahboubi A, Noorzad A (2021) Particle shape effect on internal instability of cohesionless soils. In: Proceedings of the 10th International Conference on Scour and Erosion (ICSE-10). Arlington, Virginia, USA, p 12
Milligan V (1986) Internal stability of granular filters: Discussion. Can Geotech J 23:414–418. https://doi.org/10.1139/t86-066
Nguyen NS, Taha H, Marot D (2021) A new Delaunay triangulation-based approach to characterize the pore network in granular materials. Acta Geotech. https://doi.org/10.1007/s11440-021-01157-1
Raoof A, Hassanizadeh M (2010) A new method for generating pore-network models of porous media. Transp Porous Media 81:391–407. https://doi.org/10.1007/s11242-009-9412-3
Reboul N, Vincens E, Cambou B (2008) A statistical analysis of void size distribution in a simulated narrowly graded packing of spheres. Granul Matter 10:457–468. https://doi.org/10.1007/s10035-008-0111-5

Reboul N, Vincens E, Cambou B (2010) A computational procedure to assess the distribution of constriction sizes for an assembly of spheres. Comput Geotech 37:195–206. https://doi.org/10.1016/j.compgeo.2009.09.002

Sahimi M (2011) Flow and transport in porous media and fractured rocks https://doi.org/10.1002/9783527636693

Schuler U (1996) Scattering of the composition of soils—An aspect for the stability of granular filters. In: Geofilters 96. Bitech Publications, Montreal, pp 21–34

Seblany F, Homberg U, Vincens E et al (2018) Merging criteria for defining pores and constrictions in numerical packing of spheres. Granul Matter 20:37. https://doi.org/10.1007/s10035-018-0808-z

Seblany F, Vincens E, Picault C (2021) Determination of the opening size of granular filters. Int J Numer Anal Methods Geomech 45:1195–1211. https://doi.org/10.1002/nag.3198

Sherard JL, Dunnigan LP (1986) Internal stability of granular filters: Discussion. Can Geotech J 23:418–420. https://doi.org/10.1139/t86-067

Sherard JL, Dunnigan LP, Talbot JR (1984) Basic properties of sand and gravel filters. J Geotech Eng 110:684–700. https://doi.org/10.1061/(ASCE)0733-9410(1984)110:6(684)

Shire T, O'Sullivan C (2016) Constriction size distributions of granular filters: a numerical study. Géotechnique 1–14. https://doi.org/10.1680/jgeot.15.P.215

Shire T, O'Sullivan C, Taylor HF (2016) Measurement of constriction size distributions using three grain-scale methods. Scour Eros – Proc 8th Int Conf Scour Eros 1067–1073. https://doi.org/10.1201/9781315375045-136

Silveira A (1965) An analysis of the problem of washing through in protective filters. 6th Int Conf on Soil Mechanics and Foundation Engineering, Vol. 2. University of Toronto Press, Toronto, pp 551–555

Sjah J, Vincens E (2013) Determination of the constriction size distribution of granular filters by filtration tests. Int J Numer Anal Methods Geomech 37:1231–1246. https://doi.org/10.1002/nag.2076

Skempton AW, Brogan JM (1994) Experiments on piping in sandy gravels. Géotechnique 44:449–460. https://doi.org/10.1680/geot.1994.44.3.449

Slangen P, Fannin RJ (2017) The role of particle type on suffusion and suffosion. Géotechnique Lett 7:6–10. https://doi.org/10.1680/jgele.16.00099

Sperry JM, Peirce JJ (1995) A model for estimating the hydraulic conductivity of granular material based on grain shape, grain size, and porosity. Ground Water 33:892–898. https://doi.org/10.1111/j.1745-6584.1995.tb00033.x

Tangjarusritaratorn T, Miyazaki Y, Kikumoto M, Kishida K (2022) Modeling suffusion of ideally gap-graded soil. Int J Numer Anal Methods Geomech 46:1331–1355. https://doi.org/10.1002/nag.3348

Taylor HF, O'Sullivan C, Sim WW (2015) A new method to identify void constrictions in micro-CT images of sand. Comput Geotech 69:279–290. https://doi.org/10.1016/j.compgeo.2015.05.012

Taylor HF, O'Sullivan C, Sim WW (2016) Geometric and hydraulic void constrictions in granular media. J Geotech Geoenvironmental Eng 142:. https://doi.org/10.1061/(ASCE)GT.1943-5606.0001547

Taylor HF, O'Sullivan C, Shire T, Moinet WW (2018) Influence of the coefficient of uniformity on the size and frequency of constrictions in sand filters. Géotechnique 1–29. https://doi.org/10.1680/jgeot.17.t.051

Terzaghi K, Peck RB, Mesri G (1996) Soil mechanics in engineering practice, 3rd Editio. Wiley

Vafai F (1996) Analytical modelling and laboratory studies of particle transport in filter media. Dissertation, University of Wollongong

Veiskarami M, Roshanali L, Habibagahi G (2023) A theoretical study on the hydraulic conductivity of anisotropic granular materials by implementing the microstructure tensor. Granul Matter 25:66. https://doi.org/10.1007/s10035-023-01352-9

Vincens E, Witt KJ, Homberg U (2015) Approaches to determine the constriction size distribution for understanding filtration phenomena in granular materials. Acta Geotech 10:291–303. https://doi.org/10.1007/s11440-014-0308-1

Wadell H (1933) Sphericity and roundness of rock particles. J Geol 41:310–331. https://doi.org/10.1086/624040

Wan CF, Fell R (2008) Assessing the potential of internal instability and suffusion in embankment dams and their foundations. J Geotech Geoenvironmental Eng 134:401–407. https://doi.org/10.1061/(ASCE)1090-0241(2008)134:3(401)

Witt KJ (1993) Reliability study of granular filters. In: Brauns J, Heibaum M, U. S (eds) Filters in Geotechnical and Hydraulic Engineering. Balkema: Rotterdam, pp 35–41

Wu L, Nzouapet BN, Vincens E, Bernat-minana S (2012) Laboratory experiments for the determination of the constriction size distribution of granular filters. Icse 6:233–240

Zhang L, Deng G, Chen R, Luo Z (2023) Confining stress effects on global and local responses of internal erosion in gap-graded cohesionless soils. Bull Eng Geol Environ 82:326. https://doi.org/10.1007/s10064-023-03339-5

Zheng W, Tannant DD (2017) Improved estimate of the effective diameter for use in the Kozeny-Carman equation for permeability prediction. Géotechnique Lett 7:1–5. https://doi.org/10.1680/jgele.16.00088